ISBN: 978-3-95450-214-1 ISSN: 2673-5490 doi:10.18429/JACoW-IPAC2021-THXB04

NON-INVASIVE DISPERSION FUNCTION MEASUREMENT DURING LIGHT SOURCE OPERATIONS*

B. Podobedov†, Y. Hidaka, Brookhaven National Laboratory, Upton, NY, USA

Abstract

We implemented a completely parasitic measurement of lattice dispersion functions in both horizontal and vertical planes, which is fully compatible with light source user operations. The measurement is performed by applying principal component analysis and adaptive filtering to very small residual orbit noise components introduced by the RF system and detected in the beam orbit data, sampled at 10 kHz. No changes in RF frequency are required. The measurement, performed about once a minute, was shown to be robust and immune to changes in the beam current, residual orbit noise amplitude and frequency content as well as other factors. At low current it was shown to provide similar accuracy to the standard method which shifts the RF frequency. Here we will explain our measurement technique and present typical dispersion function stability achieved during NSLS-II operations.

INTRODUCTION

Reliability and stability are arguably the two most important metrics for operating light sources. Users want X-ray beam to be there (when promised), and stable at their samples. This is why decades of effort have gone towards improving beam orbit stability [1]. More recently there is also an added emphasis on beam size stability [2]. To guarantee that the beam size at every beamline source point remains stable it would be ideal to have an on-line linear lattice characterization running during operations. This is especially important now, with light sources running user operations for many days without interruption, so there are long intervals between the routine lattice measurements (performed during machine studies) and thus a higher possibility that some subtle hardware failure may distort the lattice in the meantime.

Unfortunately, all standard lattice characterization techniques are inherently disruptive. While there has been some progress in measurements of beta-functions during light source operations [3], we are not aware of any methods to non-invasively measure the dispersion functions.

The standard method to measure the dispersion functions relies on changing the RF frequency by Δf_{RF} and measuring the difference orbits. For the horizontal plane,

$$\eta_x(s) = \alpha\big(X_0(s) - X_1(s)\big)\frac{f_{\mathrm{RF}}}{\Delta f_{\mathrm{RF}}}, \qquad (1)$$

where α is the momentum compaction. The same calculation, applied to the vertical orbits, gives $\eta_y(s)$.

The change in RF frequency needs to be large enough to provide resolvable orbit difference at low dispersion BPMs. At NSLS-II (α = 3.6e-4, f_{RF} = 500 MHz), the standard dispersion measurements shift the frequency by up to Δf_{RF} = +/-500 Hz. Multiple orbit measurements are usually performed before averaging to improve the resolution. Separately, several Δf_{RF} sub-steps are taken and η_x, η_y are found by linear fitting of equations similar to Eq. (1).

Typical NSLS-II dispersion function measurement results are shown in Fig. 1. Thirty horizontal dispersion peaks in the top plot are due to the 30-cell DBA lattice of NSLS-II. There are 180 BPMs around the ring which are used for these measurements; 60 of them (two per cell) are in high-dispersion areas, while the rest are at nominally zero dispersion locations. Nominal vertical dispersion is zero everywhere. The η_y "spikes" are due to BPM rotations. These could be measured separately and calibrated out. However, we will omit this non-essential step throughout this paper.

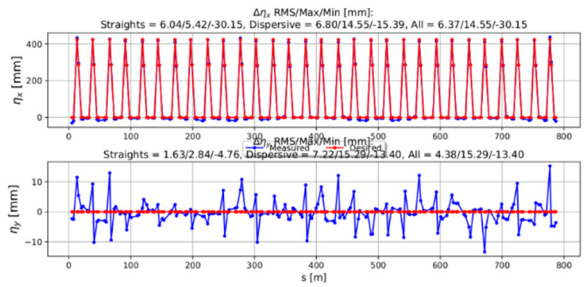

Figure 1: Typical NSLS-II dispersion function measurement results (blue) for a well-corrected lattice. Model dispersion, $\eta_{x,\,model}$ and $\eta_{y,\,model} = 0$ are shown in red.

While the standard measurement works well, it is inherently disruptive (resulting in mm-scale orbit motions) and requires the orbit feedback to be off. This measurement is typically performed during low-current studies, usually in combination with other lattice characterization tools.

NEW METHOD

We now proceed to describe our method, which is completely parasitic, does not move the beam, and can be applied with an arbitrary beam current and other machine conditions, including during user operations.

The method is based on principal component analysis (PCA), which is closely related to singular value decomposition (SVD). These techniques have a long history of successful applications to storage-ring lattice analysis (e.g. [4]), including dispersion measurements. These techniques (as well as the related independent component analysis) typically use turn-by-turn BPM data with the beam kicked by a pinger or some other excitation [5-9]. In contrast, our method uses the PCA/SVD technique for parasitic dispersion function measurement from closed orbits,

* Work supported by Brookhaven Science Associates, LLC under Contract No. DE-SC0012704 with the U.S. Department of Energy.
† boris@bnl.gov

ISBN: 978-3-95450-214-1 ISSN: 2673-5490 doi:10.18429/JACoW-IPAC2021-THXB04

which, to our knowledge, has not been demonstrated before.

We start with sampled BPM orbit data arranged in a matrix (N BPMs times M time samples, $M > N$),

$$X = \begin{pmatrix} BPM_1^x(t_1) & \cdots & BPM_1^x(t_M) \\ \vdots & \ddots & \vdots \\ BPM_N^x(t_1) & \cdots & \mathrm{BPM}_M(t_M) \end{pmatrix}. \quad (2)$$

The DC offset is subtracted from each BPM, $\widehat{X'} = X' - \overline{X'}$. Optionally, a band-pass filter (BPF) around the synchrotron frequency f_s (or other frequency band containing significant dispersive motion) is also applied,

$$\hat{X} = \mathrm{BPF}(X). \quad (3)$$

We then perform the standard SVD-decomposition into spatial (U^x) and temporal (V^x) eigenvector matrices and the eigenvalue matrix (S^x),

$$\hat{X} = U^x * S^x * V^{x\prime}, \quad (4)$$

where the eigenvectors (columns of U^x and V^x) are mutually orthogonal and square-normalized to 1. The main diagonal of S^x contains positive eigenvalues, $\lambda_1^x > \lambda_2^x \ldots > \lambda_N^x > 0$, each quantifying the amplitude of a particular spatio-temporal mode n of X. The mode's structure is completely defined by the eigenvectors U_n^x and V_n^x.

Identical steps, Eqs. (1)-(4), are performed for the vertical plane data, Y, sampled synchronously with X, to obtain λ_n^y, U_n^y and V_n^y for $n = 1, \ldots, N$.

Normalized horizontal dispersion is defined as the spatial eigenvector with the largest linear correlation coefficient with the model dispersion, $\eta_{x,model}$,

$$\tilde{\eta}_x = U_j^x, \quad j = \underset{i=1,..,N}{\mathrm{argmax}}\left(\left|corr(U_i^x, \eta_{x,model})\right|\right), \quad (5)$$

where $corr(a,b) = cov(a,b)/(\sigma_a \sigma_b)$.

Normalized dispersion in the vertical plane is defined as the eigenvector U_m^y, such that the corresponding V_m^y has the largest correlation with V_j^x, with j found in Eq. (5),

$$\tilde{\eta}_y = U_m^y, \quad m = \underset{i=1,\ldots,N}{\mathrm{argmax}}\left(corr(V_i^y, V_j^x)\right). \quad (6)$$

In words, the horizontal dispersion is the x (spatial) eigenvector which best correlates to the model dispersion. The vertical dispersion is the y spatial eigenvector whose corresponding temporal eigenvector best correlates to the temporal eigenvector for the horizontal dispersion.

The algorithm is illustrated in Fig. 2, which plots the SVD eigenvectors obtained from real data (180 BPMs sampled 1000 times at a 10 kHz rate). For simplicity, we only plot three eigenvectors with the largest eigenvalues per plane. Starting with top left figure, it is easy to spot the horizontal dispersion. Formally, however, we find it by correlating each U_n^x to the model (plotted in Fig. 1). The correlation coefficients (by absolute value) for the three vectors shown are 0.999, 0.020, and less than 0.001 for $n = 1$, 2 and 3, so the index of the dispersive mode in x-plane is $j = 1$, and $\tilde{\eta}_x = U_1^x$. Continuing counterclockwise in Fig. 2 and correlating V_1^x to each of V_n^y, we find the highest correlation with V_3^y, thus $m = 3$. Switching to space-domain we find the normalized vertical dispersion, $\tilde{\eta}_y = U_3^y$.

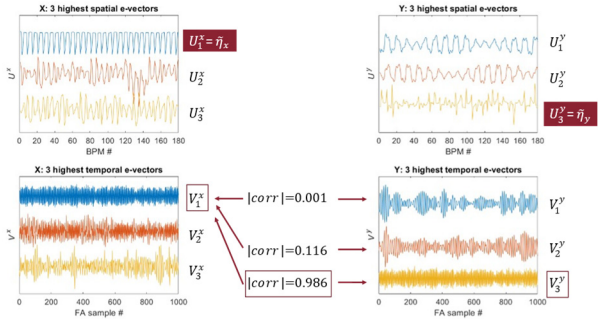

Figure 2: Normalized dispersion found from Eqs. (5) and (6); three spatial (top) and temporal (bottom) eigenvectors shown for the horizontal (left) and vertical (right) planes.

To convert the normalized dispersion functions to physics units (meters) we fit the scalar parameter κ (also in meters) to best match, in the least-squared sense, the model at dispersive BPM locations s_i, $i = 1, \ldots, 60$,

$$\kappa = \underset{\mu}{\mathrm{argmin}}\left(\sum_i \left(\mu\,\tilde{\eta}_x(s_i) - \eta_{x,model}(s_i)\right)^2\right). \quad (7)$$

Dispersion functions (at all BPMs) are then found from

$$\eta_x = \kappa\,\tilde{\eta}_x, \quad (8)$$

$$\eta_y = \kappa\,\tilde{\eta}_y \lambda_m^y / \lambda_j^x, \quad (9)$$

where j and m are the indices of the horizontal and vertical dispersive modes from Eqs. (5) and (6).

For the method to work, the orbit noise needs to have some dispersive component (energy oscillation) usually coming from the RF phase noise. However, as long as the BPMs can resolve it, this noise could be very small. For instance, at NSLS-II the total integrated rms in the bandwidth of [0.1-5000] Hz typically measures in single digit microns on dispersive BPMs, which is about 1% of the beam size (see examples in [10]). Out of that, the bulk of the energy oscillations comes in the broad peak around f_s, where the integrated noise is ~ 1 micron rms. This corresponds to the energy oscillations with $\delta E/E$ = 3e-6, which is only about 0.3% of the natural rms energy spread.

CROSS-CHECKING

To confirm the accuracy of the new method we performed many cross-checking studies against the standard method. One is illustrated in Fig. 3, which plots the results from both methods, with the data taken 15 seconds apart. For the standard method we changed f_{RF} by +/-500 Hz. For the PCA method, we recorded a 10-second-long buffer of 10 kHz orbit data. It was split into 0.1 second consecutive segments, and the PCA algorithm was applied to each. The average of these gives the dispersion function value, and +/- one standard deviation gives the error-bars, plotted in Fig. 3. Clearly, the two methods agree well with each other.

ISBN: 978-3-95450-214-1 ISSN: 2673-5490 doi:10.18429/JACoW-IPAC2021-THXB04

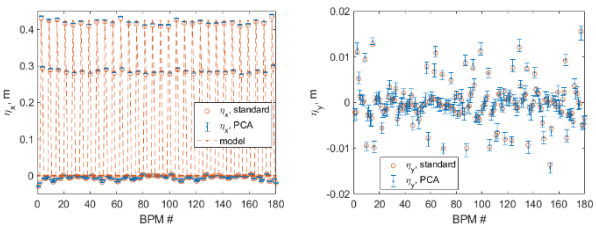

Figure 3: Dispersion functions measured with the standard and PCA-based methods at 10 mA beam current.

Other examples of cross-checking studies, including at high beam current, are presented in the accompanying talk. They all show good agreement between the two methods.

DISPERSION MEASUREMENTS DURING USER OPERATIONS

It was convenient to implement the on-line measurements of the dispersion functions by the PCA method in the so-called Orbit Monitor Input/Output Controller (IOC), which, by that time, was already in operation for a couple of years [10]. In a nutshell, about once a minute, this IOC triggers 180 BPMs, acquires 10 seconds of 10 kHz (FA) orbit data, extracts various orbit-stability-related quantities, and writes them into EPICS PVs. We added the dispersion calculations, Eqs. (2)-(9), to be performed on the same BPM data with the results for η_x and η_y written into PVs. This allowed us to monitor the dispersion functions during operations alongside of other machine PVs.

Having operated this IOC with the added dispersion measurement for about a year, we generally found the dispersion functions to be very stable during regular topoff operations. Over this time, we had instances of operations with varying beam currents, RF system settings, orbit feedback settings, etc.; all of these substantially affecting the amount and spectral content of the residual orbit noise. In all instances, our dispersion measurement performed well.

One of these events, from 11/24/2019, is illustrated in Fig. 4. Here, due to injector problems, topoff was disabled, and operations continued in decay mode. Beam current decayed from 400 mA to 290 mA over ~ 4 hours; 400 mA topoff injections resumed afterwards. During this time the total noise on dispersive BPMs in [0.1-5000] Hz bandwidth was changing by a factor of >2. The highest spectral peak's amplitude was changing by a factor >10, while its frequency was hopping between 720 Hz and f_s ~ 2 kHz (see talk, page 19). Nevertheless, as indicated by largely overlapping traces in Fig. 4, η_x and η_y remained quite stable.

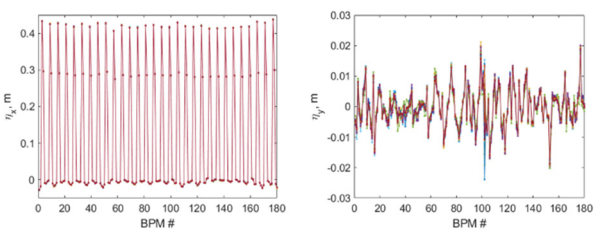

Figure 4: η_x and η_y (446 traces each) measured every 2 minutes over ~ 15 hours, 4 of which were in decay mode.

Finally, we present an example of a significant change of the dispersion functions that occurred during the 2nd week of March 2020. That week's operations started on 3/11/2020 at noon. Users were provided with uninterrupted 400 mA beam until a beam dump occurred about three days later. The cause of the dump (beamline PPS glitch) was unrelated to the storage ring. The beam was restored in about one hour and uninterrupted operations continued until the planned shutdown for interlock checks on 3/20/2020, 08:00. Dispersion functions, measured continuously during that week, are plotted in Fig. 5. Clearly, they were very stable (traces largely overlap), both before (top subplot) and after the dump (bottom subplot). (We only plot η_x but the same was checked to be true for η_y). However, the before and after sets of dispersion functions differ significantly, indicating a dispersion error, inadvertently introduced during machine recovery. Note that this error was undetected by other available diagnostics, which demonstrates the value of continuous dispersion measurements during user operations.

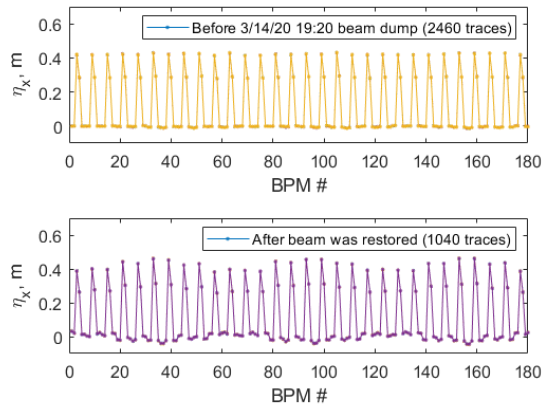

Figure 5: η_x measured every 2 minutes over 5 days of operations, before (top) and after 3/14/2020 beam dump.

CONCLUSION

We implemented a completely parasitic measurement of lattice dispersion functions in both horizontal and vertical planes, which is fully compatible with light source user operations. The measurement is performed by applying principal component analysis to very small residual orbit noise components (passively introduced by the RF system) detected in the beam orbit data. The measurement was shown to be robust and immune to changes in beam current, residual orbit noise amplitude and frequency content and other factors. Extensive cross-checking has revealed that our method provides similar accuracy to the traditional method which shifts the RF frequency. Measurements during NSLS-II operations confirmed dispersion to be very stable.

We believe our method can be implemented at other light sources which can capture reasonably long orbit buffers with BPM sampling rates faster than the synchrotron frequency.

We are thankful to Anton Derbenev and Kiman Ha for implementing Orbit Monitor IOC as well as to Robert Rainer for help with the CSS Control Panels.

ISBN: 978-3-95450-214-1 ISSN: 2673-5490 doi:10.18429/JACoW-IPAC2021-THXB04

REFERENCES

[1] G. M. Wang, "Advances in Beam Stability in Low-Emittance Synchrotron Light Sources", presented at the 12th Int. Particle Accelerator Conf. (IPAC'21), Campinas, Brazil, May 2021, paper FRXA02, this conference.

[2] S. C. Leemann *et al.*, "Demonstration of machine learning-based model-independent stabilization of source properties in synchrotron light sources", *Phys. Rev. Lett.*, vol. 123, p. 194801, 2019. doi:10.1103/PhysRevLett.123.194801

[3] W. Cheng, K. Ha, Y. Li, and B. Podobedov, "Beam position monitor gate functionality implementation and applications", *MethodsX*, vol. 5, pp. 626–634, 2018. doi:10.1016/j.mex.2018.06.006

[4] R. Tomás, M. Aiba, A. Franchi, and U. Iriso, "Review of linear optics measurement and correction for charged particle accelerators", *Phys. Rev. Accel. Beams*, vol. 20, p. 054801, 2017. doi:10.1103/PhysRevAccelBeams.20.054801

[5] C. X. Wang, V. Sajaev, and C. Y. Yao, "Phase advance and β function measurements using model-independent analysis", *Phys. Rev. ST Accel. Beams*, vol. 6, p. 104001, 2003. doi:10.1103/PhysRevSTAB.6.104001

[6] A.V. Petrenko, A. A. Valishev, and V. A. Lebedev, "Model-independent analysis of the Fermilab Tevatron turn-by-turn beam position monitor measurements", *Phys. Rev. ST Accel. Beams*, vol. 14, p. 092801, 2011. doi:10.1103/PhysRevSTAB.14.092801

[7] X. Huang, S. Y. Lee, E. Prebys, and R. Tomlin, "Application of independent component analysis to Fermilab Booster", *Phys. Rev. ST Accel. Beams*, vol. 6, p. 104001, 2005. doi:10.1103/PhysRevSTAB.8.064001

[8] F. Wang and S.Y. Lee, "Vertical-beam emittance correction with independent component analysis method", *Phys. Rev. ST Accel. Beams*, vol. 11, p. 050701, 2008. doi:10.1103/PhysRevSTAB.11.050701

[9] X. Yang and X. Huang, "A method for simultaneous linear optics and coupling correction for storage rings with turn-by-turn beam position monitor data", *Nucl. Instrum. Methods Phys. Res., Sect. A*, vol. 828, pp. 97–104, 2016. doi:10.1016/j.nima.2016.05.020

[10] B. Podobedov, A. A. Derbenev, K. Ha, and T. V. Shaftan, "Continuous Monitoring of Spectral Features of Electron Beam Orbit Motion at NSLS-II", in *Proc. North American Particle Accelerator Conf. (NAPAC2019)*, Lansing, MI, USA, Sep. 2019, pp. 673-676. doi:10.18429/JACoW-NAPAC2019-WEPLM05